The Astrophysical Journal, 707:L102–L106, 2009 December 10 doi:10.1088/0004-637X/707/1/L102

THE LARGEST GRAVITATIONAL LENS: MACS J0717.5+3745 ($z = 0.546$)

Adi Zitrin, Tom Broadhurst, Yoel Rephaeli, and Sharon Sadeh
School of Physics and Astronomy, Tel Aviv University, Israel
Received 2009 July 24; accepted 2009 November 13; published 2009 November 30

ABSTRACT

We identify 13 sets of multiply-lensed galaxies around MACS J0717.5+3745 ($z = 0.546$), outlining a very large tangential critical curve of major axis $\sim 2\farcm8$, filling the field of the *Hubble Space Telescope*/Advanced Camera for Surveys. The equivalent circular Einstein radius is $\theta_e = 55'' \pm 3''$ (at an estimated source redshift of $z_s \sim 2.5$), corresponding to $r_e \simeq 350 \pm 20$ kpc at the cluster redshift, nearly three times greater than that of A1689 ($r_e \simeq 140$ kpc for $z_s = 2.5$). The mass enclosed by this critical curve is very large, $7.4 \pm 0.5 \times 10^{14}\ M_\odot$ and only weakly model dependent, with a relatively shallow mass profile within $r < 250$ kpc, reflecting the unrelaxed appearance of this cluster. This shallow profile generates a much higher level of magnification than the well-known relaxed lensing clusters of higher concentration, so that the area of sky exceeding a magnification of >10 times, is $\simeq 3.5\square'$ for sources with $z \simeq 8$, making MACS J0717.5+3745 a compelling target for accessing faint objects at high redshift. We calculate that only one such cluster, with $\theta_e \geqslant 55''$, is predicted within $\sim 10^7$ Universes with $z \geqslant 0.55$, corresponding to a virial mass $\geqslant 3 \times 10^{15}\ M_\odot$, for the standard ΛCDM (*WMAP5* parameters with 2σ uncertainties).

Key words: dark matter – galaxies: clusters: individual (MACS J0717.5+3745) – gravitational lensing

1. INTRODUCTION

Improvements in gravitational-lensing modeling together with the fabulous image quality of the Advanced Camera for Surveys (ACS) have led to the identification of increasing numbers of multiply-lensed images and the discovery of some surprisingly large lenses (e.g., Kneib et al. 1996; Broadhurst et al. 2005; Bradač et al. 2008; Halkola et al. 2008; Liesenborgs et al. 2008; Limousin et al. 2008; Zitrin et al. 2009; Zitrin & Broadhurst 2009).

The largest bound structures to form hierarchically are likely to have collapsed recently and hence should be found relatively locally, at low redshifts. The larger volume available with increasing distance means that in practice we cannot expect to reside next to the most massive cluster. The Coma cluster, $z = 0.023$, is the most massive "local" cluster with a reliable weak lensing based mass of $M_{\rm vir} \sim 0.65 \times 10^{15}\ M_\odot$ (Gavazzi et al. 2009), similar to earlier dynamical estimates $\sim 0.8 \times 10^{15}\ M_\odot$ (The & White 1986; Geller et al. 1999). Other more distant clusters are known from lensing to be more massive, such as A2218 at $z = 0.16$ (Kneib et al. 1996) and A1689 at $z = 0.18$, with $1.6 \pm 0.2 \times 10^{15}\ M_\odot$ (Broadhurst et al. 2005; Umetsu & Broadhurst 2008), superseded by the most distant Abell cluster, A370 at $z = 0.37$ and the most luminous X-ray cluster RXJ1347, $z = 0.45$, with masses reliably determined from weak lensing distortion and magnification of $\simeq 2 \times 10^{15}\ M_\odot$ (Broadhurst et al. 2008).

Strong lensing is not seen for low redshift clusters ($z < 0.15$) because the central projected mass densities do not exceed the critical density required to generate a sizable Einstein radius, which scales inversely with lens distance, diverging at low redshift. Similarly, at high redshift as the lens distance approaches that of the distant sources, thus the critical density is too great for strong lensing. Geometrically, lensing is optimized at intermediate redshifts, where for a given mass the critical density for lensing is minimal, but this is partly offset by the late hierarchical growth of high-mass systems. This trade-off results in estimates of the amplitude of strong lensing to favor the redshift range $z = 0.2$–0.4, for Navarro–Frenk–White (NFW) like mass profiles (Broadhurst & Barkana 2008; Oguri & Blandford 2009). Seemingly, all rich and X-ray luminous clusters at modest redshift are found to have many multiply-lensed images when examined with sufficient depth and resolution, implying that the mass profiles of clusters are in general sufficiently peaked that the critical density for lensing is exceeded.

The Einstein radii of the most massive clusters seem to be larger than predicted by the ΛCDM model (Broadhurst & Barkana 2008; Puchwein & Hilbert 2009), based on the "Millenium" simulation (Springel et al. 2005). This discrepancy is empirically supported by the surprisingly concentrated mass profiles measured for such clusters, when combining the inner strong lensing with the outer weak lensing signal (Gavazzi et al. 2003; Broadhurst et al. 2005, 2008; Limousin et al. 2008; Donnarumma et al. 2009; Oguri et al. 2009; Umetsu et al. 2009; Zitrin et al. 2009).

These largest lensing clusters have proven to be excellent targets for accessing the faint early universe due to their large magnification consistently providing the highest redshift galaxies (Ebbels et al. 1996; Franx et al. 1997; Frye & Broadhurst 1998; Bouwens et al. 2004; Kneib et al. 2004; Bradley et al. 2008; Zheng et al. 2009; see also Broadhurst et al. 1995). The larger sizes of lensing images has provided increased spatial detail and the large magnifications permit observations of increased spectral resolution, leading to the discovery that metal-enriched material is typically outflowing from galaxies at $z > 4$ (Franx et al. 1997; Frye & Broadhurst 1998; Frye et al. 2002).

With the goal of discovering high redshift galaxies and to better define the mass profiles of galaxy clusters in general, we have combined data for a sample of well-studied clusters. In this process, we have uncovered the extreme lensing properties of MACS J0717.5+3745 ($z = 0.546$), a cluster originally identified in the highly complete sample of the most X-ray luminous clusters in the universe (Ebeling et al. 2004, 2007). This cluster is thought to be amongst the most massive clusters known, forming part of an intricate dark matter (DM) filamentary structure of ~ 4 Mpc (Ebeling et al. 2004; Ma et al. 2008), whose complex X-ray emission indicates ongoing merging (Ma et al. 2009) accompanied by the most powerful

known radio halo (van Weeren et al. 2009; Bonafede et al. 2009).

In Section 2, we describe the observations; the lensing analysis is described in Section 3; our results are presented in Section 4 and in Section 5 we discuss and conclude them. Throughout the Letter, we adopt the standard cosmology ($\Omega_{m0} = 0.3$, $\Omega_{\Lambda 0} = 0.7$, $h = 0.7$). Accordingly, one arcsecond corresponds to 6.42 kpc/h_{70} at the redshift of this cluster. The reference center of our analysis is fixed near the center of the ACS frame at R.A. = 07:17:31.65, decl. = +37:45:03.12 (J2000.0).

2. OBSERVATIONS

The very X-ray luminous cluster MACS J0717.5+3745, which is the denser northwestern region of the large-scale filament found by Ebeling et al. (2004), was imaged in 2004 April and in 2005 and 2006 October, with the Wide Field Channel (WFC) of the ACS installed on the *Hubble Space Telescope* (*HST*). Integration times of ∼4500 s were obtained through each of the F555W and the F814W filters in the 2004 April run. We retrieved these images from the Hubble Legacy Archive, along with a subsequent exposure in the F606W band (2005 January, integration time of 1980 s) to form a composite high-resolution three-color image. Several obvious close pairs of multiply-lensed galaxies and giant arcs are immediately visible throughout the full frame, with which we begin our modeling process described below.

3. LENSING ANALYSIS

We apply our well-tested approach to lens modeling, which we have applied successfully to A1689, Cl0024, and MACS J1149.5+2223, uncovering large numbers of multiply-lensed images in several clusters imaged with *HST*/ACS (Broadhurst et al. 2005; Zitrin et al. 2009; Zitrin & Broadhurst 2009). The full details of this approach can be found in these papers. Briefly, the basic assumption adopted is that mass approximately traces light, so that the photometry of the red cluster member galaxies is the starting point for our model.

Cluster member galaxies are identified as lying close to the cluster sequence by the photometry provided in the Hubble Legacy Archive. We approximate the large-scale distribution of matter by assigning a power-law mass profile to each galaxy, the sum of which is then smoothed. The degree of smoothing and the index of the power law are the main free parameters. A worthwhile improvement in fitting the location of the lensed images is generally found by expanding to first order the gravitational potential of the smooth component, equivalent to a coherent shear describing the overall matter ellipticity, where the direction of the shear and its amplitude are free, allowing for some flexibility in the relation between the distribution of DM and the distribution of galaxies, which cannot be expected to trace each other in detail. The total deflection field $\vec{\alpha}_T(\vec{\theta})$, consists of the galaxy component, $\vec{\alpha}_{\rm gal}(\vec{\theta})$, scaled by a factor $K_{\rm gal}$, the cluster DM component $\vec{\alpha}_{\rm DM}(\vec{\theta})$, scaled by $(1 - K_{\rm gal})$, and the external shear component $\vec{\alpha}_{\rm ex}(\vec{\theta})$:

$$\vec{\alpha}_T(\vec{\theta}) = K_{\rm gal}\vec{\alpha}_{\rm gal}(\vec{\theta}) + (1 - K_{\rm gal})\vec{\alpha}_{\rm DM}(\vec{\theta}) + \vec{\alpha}_{\rm ex}(\vec{\theta}), \quad (1)$$

where the deflection field at position $\vec{\theta}_m$ due to the external shear, $\vec{\alpha}_{\rm ex}(\vec{\theta}_m) = (\alpha_{{\rm ex},x}, \alpha_{{\rm ex},y})$, is given by

$$\alpha_{{\rm ex},x}(\vec{\theta}_m) = |\gamma|\cos(2\phi_\gamma)\Delta x_m + |\gamma|\sin(2\phi_\gamma)\Delta y_m, \quad (2)$$

$$\alpha_{{\rm ex},y}(\vec{\theta}_m) = |\gamma|\sin(2\phi_\gamma)\Delta x_m - |\gamma|\cos(2\phi_\gamma)\Delta y_m, \quad (3)$$

where $(\Delta x_m, \Delta y_m)$ is the displacement vector of the position $\vec{\theta}_m$ with respect to a fiducial reference position, which we take as the lower left pixel position (1, 1), and ϕ_γ is the position angle of the spin-2 external gravitational shear measured counterclockwise from the x-axis.

We lens candidate galaxies back to the source plane using the derived deflection field, and then re-lens this source plane to predict the detailed appearance and location of additional counter images (see Figures 1 and 2), which are then searched for in the data. The fit is assessed by the rms uncertainty in the image plane:

$${\rm rms}^2_{\rm images} = \sum_i ((x_i^{'} - x_i)^2 + (y_i^{'} - y_i)^2)/N_{\rm images}, \quad (4)$$

where $x_i^{'}$ and $y_i^{'}$ are the locations given by the model, and x_i and y_i are the real images location, and the sum is over all $N_{\rm images}$ images.

Importantly, this image-plane minimization does not suffer from the well-known bias involved with source plane minimization which biasses solutions toward high magnification and hence correspondingly shallower profiles. The model is successively refined as additional sets of multiple images are identified and incorporated to improve the fit (Zitrin et al. 2009). In addition, we find that a bright foreground elliptical galaxy (R.A. = 07:17:37.16, decl. = +37:44:22.54) is important to include in the model as it locally affects lensed images in the eastern to central part of the ACS frame, including their relative lensing distance.

In the above process we uncovered and used 34 multiply-lensed images, corresponding to 13 lensed background galaxies, to constrain the mass distribution and profile of this cluster. A lensed pair of red drop-out objects which are not seen in the F555W band at an estimated redshift of $z \sim 4$ (system number 5, see Figure 1), helps us pin down accurately the normalization of the deflection field by adopting the lensing distance for this redshift which is nearly independent of cosmology (see also Broadhurst et al. 2005; Zitrin et al. 2009). The image-plane rms of our final model is very good, 2.″2 per image, whereas for comparison, in A1689 an rms of 3.″2 was achieved by Broadhurst et al. (2005) and for Cl0024 an rms of 2.″5 was achieved by Zitrin et al. (2009).

4. RESULTS

The derived surface mass distribution is relatively shallow (see Figure 3) in accordance with the unrelaxed appearance of this cluster, which is known to be in the process of merging, with disturbed X-ray emission, hot shocked regions (Ma et al. 2008, 2009), and powerful radio halo emission (van Weeren et al. 2009; Bonafede et al. 2009). We find that the elongated central distribution of galaxies is followed by a very extended tangential critical curve, enclosing a large critically lensed region of $\simeq 2.63\square'$ with an equivalent Einstein radius of $\sim 55'' \pm 3.''0$ (for an estimated source redshift of $z \sim 2.5$). This corresponds to a physical scale of 350 ± 20 kpc/h_{70}, substantially larger than in any other known cluster. This very large radius adds to the already uncomfortable discrepancy between the large Einstein radii observed for massive clusters and the predictions based on the standard ΛCDM cosmology (Broadhurst & Barkana 2008; Sadeh & Rephaeli 2008; Puchwein & Hilbert 2009) for which such large Einstein radii can only be contemplated with mass

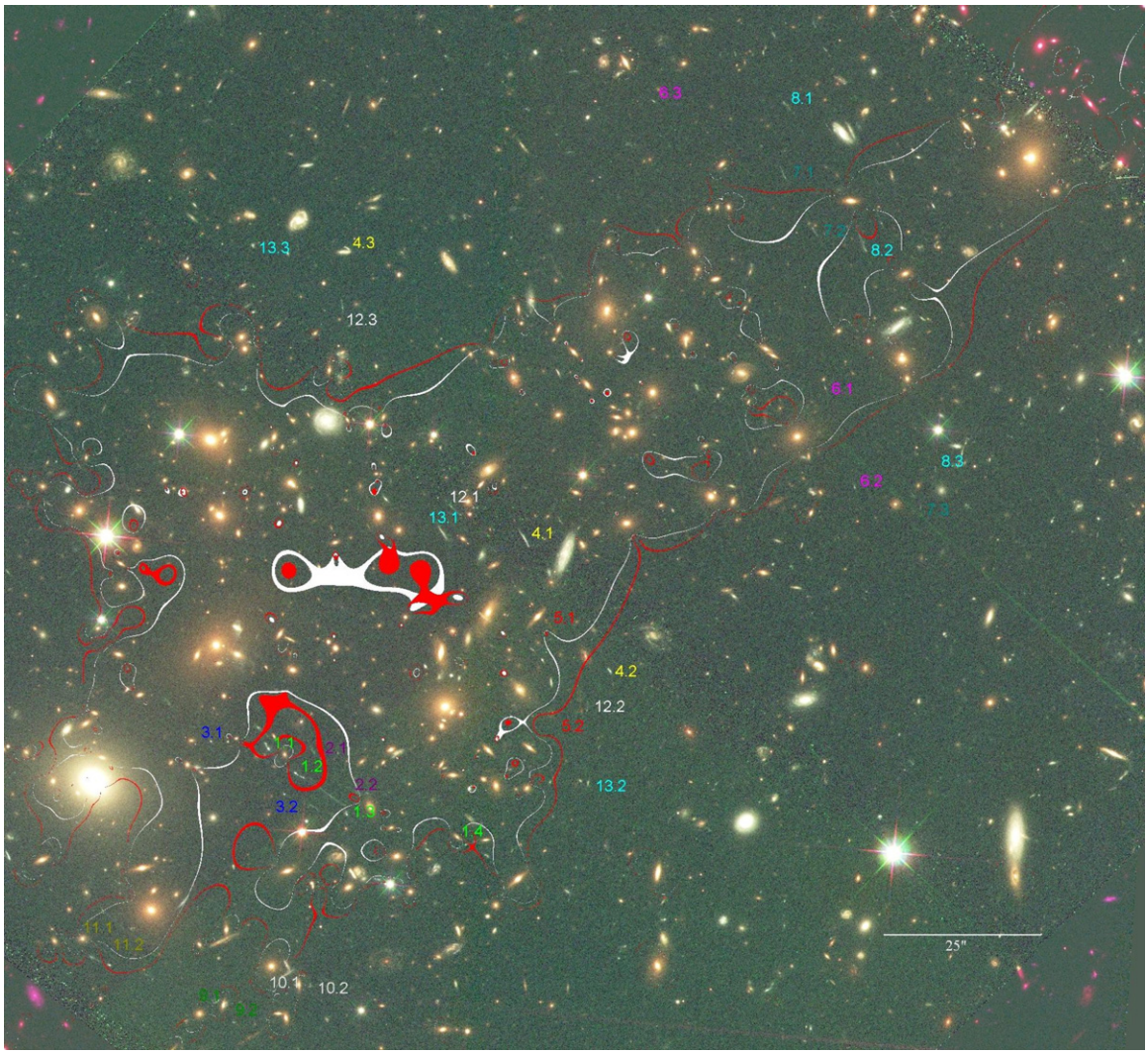

Figure 1. Cluster MACS J0717.5+3745 ($z = 0.546$) imaged with *HST*/ACS F555W, F606W, and F814W bands. The 34 multiply lensed images identified by our model are numbered here. The white curve overlaid shows the tangential critical curve corresponding to the distance of system 1 at an estimated redshift of $z \sim 2.5$, and which passes through several close pairs of lensed images in this system. The larger critical curve overlaid in red corresponds to the larger source distance for the red dropout galaxy number 5, at the estimated photometric redshift of $z \sim 4$. This large tangential critical curve encloses a very large lensed region equivalent to ~400 kpc in radius at the redshift of the cluster, $z = 0.546$.

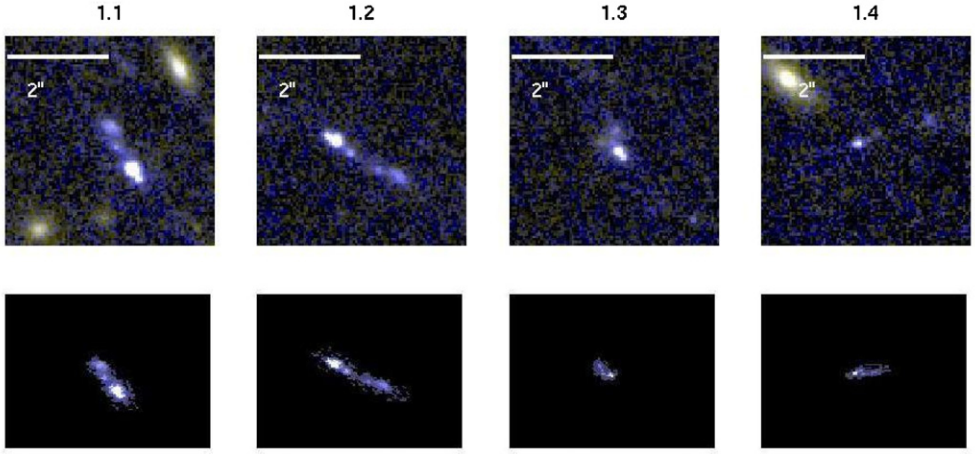

Figure 2. Reproduction of system 1 by our model. The observed images are shown in the top row are compared with our model generated images below. Each model image is generated using as input the pixels of image 1.1 (except for the model image of 1.1 which is generated by relensing the observed image 1.2) and delensing these pixels back to the source plane and then relensing the source plane to generate the counter images. It is clear that our model is successful in demonstrating the multiply-lensed relation between the four observed images.

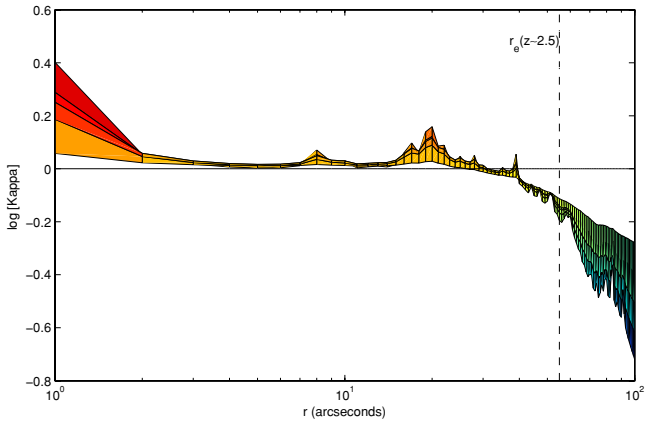

Figure 3. Radial surface mass density profile, $\kappa(r)$, in units of the critical surface density, i.e. $\kappa(r) = \Sigma(r)/\Sigma_{\rm crit}$, derived for the range of radius covered by all sets of multiple images shown in Figure 2. The profile is shallow within ∼250 kpc, at a level close to the critical density for system 1 (black line). The vertical dashed line at ∼55″ is the Einstein radius at the redshift of system 1. This profile was measured circularly while centered on the central pixel of the 2D mass distribution shown in Figure 4.

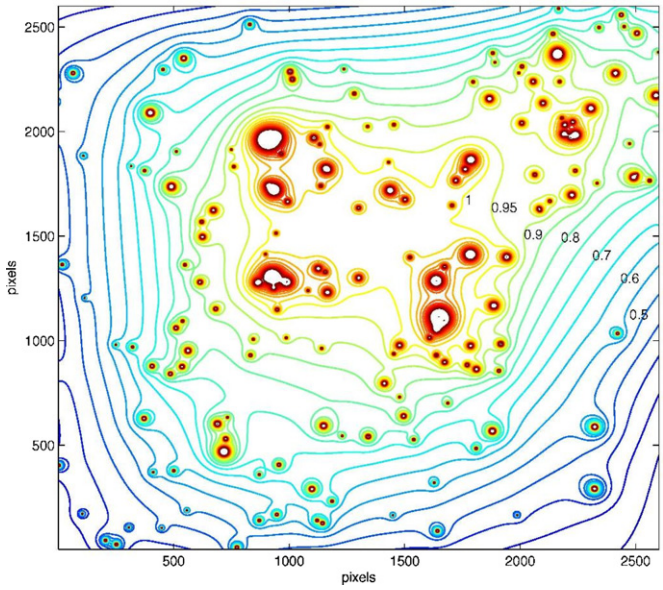

Figure 4. Zoomed-in 2D surface mass distribution (κ), in units of the critical density. Contours are shown in linear units, derived from the mass model constrained using 34 multiply-lensed images seen in Figure 2. The axes are in ACS pixels. Note that the central mass distribution of is rather flat reflecting the unrelaxed appearance of this cluster.

distributions which are highly prolate and aligned along the line of sight (Corless & King 2007; Oguri & Blandford 2009). Instead, here this cluster is evidently elongated across the line of sight, traced by the distribution of member galaxies, and by the extended X-ray emission and the tangential curves (see Figure 1).

Naturally, such a comparison is biased by the asymmetry and shape of the critical curve, which cannot be perfectly compared with DM simulations. However, this difference is small, as we find that a circularly symmetric lens of $\theta_E = 55''$, centered on the center of Figure 4, contains $6.8 \times 10^{14}\,M_\odot$, 92% of the mass contained within the tangential critical curve (for $z_s = 2.5$).

The mass enclosed within the tangential critical curve, for $z_s = 2.5$, is very high $7.4 \pm 0.5 \times 10^{14}\,M_\odot$. The mass enclosed within the larger critical curve for the multiply-lensed dropout

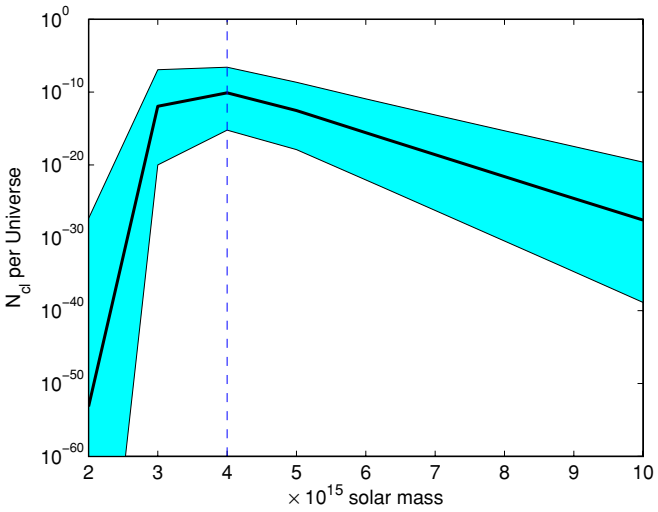

Figure 5. Number of clusters per universe with masses exceeding M, lying at redshift $z \geqslant 0.55$, for which the predicted Einstein radius is $\theta \geqslant 55 \pm 3''$. The shaded area reflects the variance generated by incorporating into the ΛCDM model the 2σ uncertainty in the cosmological parameters h, n, and σ_8, about the *WMAP*5 values, and also the 1σ uncertainty in the measured θ_E. This number peaks near $M \sim 4 \times 10^{15}\,M_\odot$, with $N_{\rm cl} \sim 2.7 \times 10^{-7}$.

galaxy, number 5, at an estimated source redshift of $z \sim 4$ is correspondingly larger, $\simeq 1.0 \times 10^{15}\,M_\odot$ (marked in red, Figure 1). Clearly, the total mass associated with this cluster cannot be smaller than this and is likely to be several times larger, and may soon be reliably estimated from weak lensing. We stress that the scale of the tangential critical curve hardly depends on the mass profile because it is set by the critical density for lensing, which depends only on fundamental constants and the distances involved, so that different profiles explored in the modeling procedure yield very similar critical curves, and hence similarly large Einstein radii and an accurate enclosed mass.

5. DISCUSSION AND CONCLUSIONS

Theoretically, we can make an approximate estimate of the probability of obtaining such a cluster in the context of the tightly proscribed ΛCDM model. Using the probability distribution function (PDF) of halo formation times, calculated within the framework of the extended Press & Schechter (EPS) formalism (Lacey & Cole 1993), we derived a corresponding PDF of halo concentration parameters (Sadeh & Rephaeli 2008) by adopting the formation redshift-concentration scaling, deduced by Wechsler et al. (2002), from *N*-body simulations.

Solving the equation governing the relation between the concentration parameter and θ_E assuming an NFW profile (e.g., Broadhurst & Barkana 2008), leads to a PDF of Einstein radii. Here we adopt the mean source redshift $z_s = 2.5$ as described above. The product of the Press & Schechter mass function abundance of clusters within the relevant mass and redshift ranges with the cumulative Einstein radius probabilities multiplied by the volume available at $z > 0.55$ provides the number of clusters expected above this redshift for standard ΛCDM where we allow for 2σ uncertainty in the *WMAP*5 values of the parameters $[n, h, \sigma_8]$). Extremely low numbers of clusters are predicted peaking at $M \simeq 4 \times 10^{15} M_\odot$ with a maximum probability of only 2.7×10^{-7} objects per universe (see Figure 5), or approximately half this value when allowing for the area of sky covered by the *ROSAT* all-sky survey. This comparison with ideal DM halos is made somewhat uncertain

by the observed asymmetry of the central mass distribution. However, as noted in Section 4, there is only an 8% difference between the mass within the critical area and the mass within the circular equivalent critical area derived from our model, whereas the discrepancy with theory is orders of magnitude. Clearly it is important to obtain the total mass of the cluster via weak lensing which we are now estimating but it is reasonable to suppose this lies close to the most probable value derived crudely here, given that the mass interior to the critical curve is already 25% of this value.

MACS J0717.5+3745 is the second strong-lensing analyzed cluster (along the recent critically convergent lens MACS J1149.5+2223, Zitrin & Broadhurst 2009) out of several other very luminous X-ray clusters uncovered by Ebeling et al. (2007) in the *ROSAT* all-sky survey. Both these clusters have unconcentrated central galaxy distributions reflecting their unrelaxed state and for which we have shown that the central mass distribution is likewise very unconcentrated. A relatively shallow mass profile boosts the gravitational lens magnification and we calculate that the total area of sky exceeding a magnification, $\mu > 10$, is $\sim$3.5 arcmin^2, corresponding to the current high redshift limit of $z \sim 8$, which is far higher than the equivalent area calculated for other massive clusters (Broadhurst et al. 2005; Zitrin et al. 2009). Such unrelaxed and massive clusters open a potentially new regime of highly magnifying lenses for accessing the faint distant universe.

We thank an anonymous referee for useful comments. This research is supported by the Israel Science Foundation grant 1400/10. ACS was developed under NASA contract NAS 5-32865. This research is based on observations provided in the Hubble Legacy Archive, which is a collaboration between the Space Telescope Science Institute (STScI/NASA) and the Space Telescope European Coordinating Facility (ST-ECF/ESA) and the Canadian Astronomy Data Centre (CADC/NRC/CSA).

REFERENCES

Bonafede, A., et al. 2009, A&A, 503, 707
Bouwens, R. J., et al. 2004, ApJ, 616, 79
Bradač, M., et al. 2008, ApJ, 681, 187
Bradley, L. D., et al. 2008, ApJ, 678, 647
Broadhurst, T. J., & Barkana, R. 2008, MNRAS, 390, 1647
Broadhurst, T. J., Taylor, A. N., & Peacock, J. A. 1995, ApJ, 438, 49
Broadhurst, T., Umetsu, K., Medezinski, E., Oguri, M., & Rephaeli, Y. 2008, ApJ, 685, L9
Broadhurst, T., et al. 2005, ApJ, 621, 53
Corless, V. L., & King, L. J. 2007, MNRAS, 380, 149
Donnarumma, A., Ettori, S., Meneghetti, M., & Moscardini, L. 2009, MNRAS, 398, 438
Ebbels, T. M. D., Le Borgne, J.-F., Pello, R., Ellis, R. S., Kneib, J.-P., Smail, I., & Sanahuja, B. 1996, MNRAS, 281, 75
Ebeling, H., Barrett, E., & Donovan, D. 2004, ApJ, 609L, 49
Ebeling, H., et al. 2007, ApJ, 661, 33
Franx, M., Illingworth, G. D., Kelson, D. D., van Dokkum, P. G., & Tran, K. 1997, ApJ, 486, 75
Frye, B., & Broadhurst, T. 1998, ApJ, 499, 115
Frye, B., Broadhurst, T., & Benítez, N. 2002, ApJ, 568, 558
Gavazzi, R., Fort, B., Mellier, Y., Pello, R., & Dantel-Fort, M. 2003, A&A, 403, 11
Gavazzi, R., Adami, C., Durret, F., Cuillandre, J.-C., Ilbert, O., Mazure, A., Pelló, R., & Ulmer, M. P. 2009, A&A, 498L, 33
Geller, M. J., Diaferio, A., & Kurtz, M. J. 1999, ApJ, 517L, 23
Halkola, A., et al. 2008, A&A, 481, 65
Kneib, J.-P., Ellis, R. S., Santos, M. R., & Richard, J. 2004, ApJ, 607, 697
Kneib, J.-P., Ellis, R. S., Smail, I., Couch, W. J., & Sharples, R. M. 1996, ApJ, 471, 643
Lacey, C., & Cole, S. 1993, MNRAS, 262, 627
Liesenborgs, J., de Rijcke, S., Dejonghe, H., & Bekaert, P. 2008, MNRAS, 389, 415
Limousin, M., et al. 2008, A&A, 489, 23
Ma, C.-J., Ebeling, H., & Barrett, E. 2009, ApJ, 693L, 56
Ma, C.-J., Ebeling, H., Donovan, D., & Barrett, E. 2008, ApJ, 684, 160
Oguri, M., & Blandford, R. D. 2009, MNRAS, 392, 930
Oguri, M., et al. 2009, ApJ, 699, 1038
Puchwein, E., & Hilbert, S. 2009, MNRAS, 398, 1298
Sadeh, S., & Rephaeli, Y. 2008, MNRAS, 388, 1759
Springel, V., et al. 2005, Nature, 435, 629
The, L. S., & White, S. D. M. 1986, AJ, 92, 1248
Umetsu, K., & Broadhurst, T. 2008, ApJ, 684, 177
Umetsu, K., et al. 2009, ApJ, submitted (arXiv:0908.0069)
van Weeren, R. J., Rottgering, H. J. A., Bruggen, M., & Cohen, A. 2009, A&A, 505, 991
Wechsler, R. H., Bullock, J. S., Primack, J. R., Kravtsov, A. V., & Dekel, A. 2002, ApJ, 568, 52
Zheng, W., et al. 2009, ApJ, 697, 1907
Zitrin, A., & Broadhurst, T. 2009, ApJ, 703, L132
Zitrin, A., et al. 2009, MNRAS, 396, 1985